# Pure Spin Current Injection in Hydrogenated Graphene Structures

Reinaldo Zapata-Peña[1], Bernardo S. Mendoza[1], Anatoli I. Shkrebtii[2]

[1]*Centro de Investigaciones en Óptica, León, Guanajuato 37150, México and*

[2]*University of Ontario, Institute of Technology, Oshawa, ON, L1H 7L7, Canada*

(Dated: July 1, 2017)

Lorem ipsum dolor sit amet, consectetuer adipiscing elit. Etiam lobortis facilisis sem. Nullam nec mi et neque pharetra sollicitudin. Praesent imperdiet mi nec ante. Donec ullamcorper, felis non sodales commodo, lectus velit ultrices augue, a dignissim nibh lectus placerat pede. Vivamus nunc nunc, molestie ut, ultricies vel, semper in, velit. Ut porttitor. Praesent in sapien. Lorem ipsum dolor sit amet, consectetuer adipiscing elit. Duis fringilla tristique neque. Sed interdum libero ut metus. Pellentesque placerat. Nam rutrum augue a leo. Morbi sed elit sit amet ante lobortis sollicitudin. Praesent blandit blandit mauris. Praesent lectus tellus, aliquet aliquam, luctus a, egestas a, turpis. Mauris lacinia lorem sit amet ipsum. Nunc quis urna dictum turpis accumsan semper.

## I. INTRODUCTION

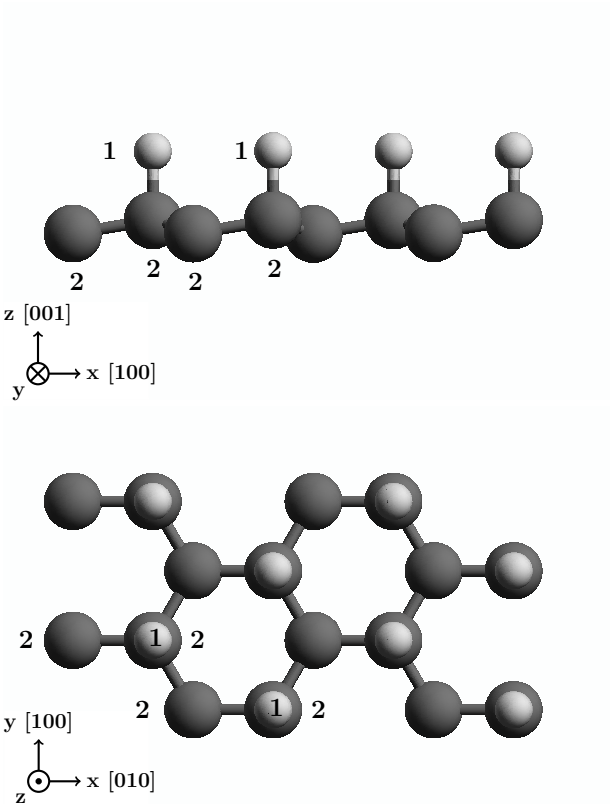


FIG. 1. Up structure

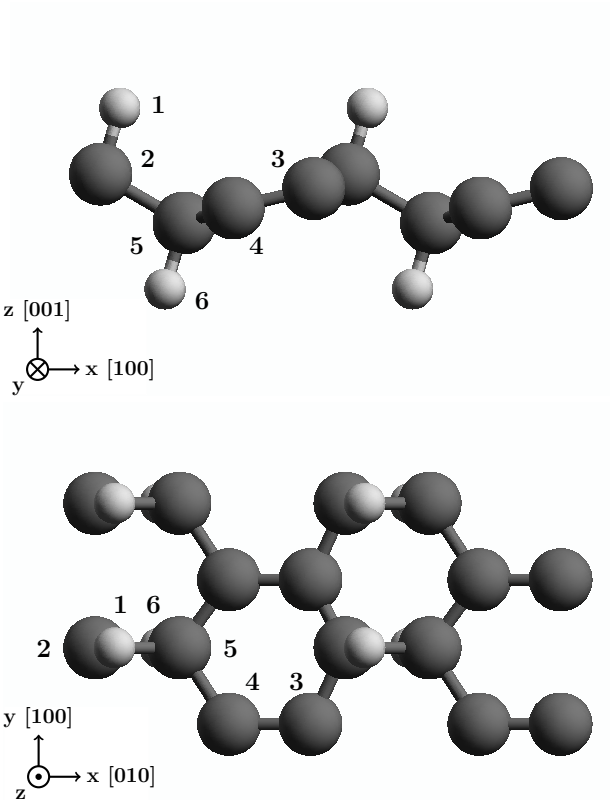


FIG. 2. Alt structure.

Spintronics is an emerging research field of electronics in which the manipulation and transport of spin of electrons in a solid state media plays the determining role adding a new degree of freedom to the conventional charge manipulation.[1,2] At present there is an increasing interest in attain the same level of control over the transport of spin at micro or nano scales as has been done for the flow of charge in typical electronic devices.[3] Some semiconductor spin-

tronics devices have been proposed[4–7] and some of them require spin polarized electrical current[8] or pure spin current (PSC). One of the difficulties to achieve the development of spin current and PSC semiconductor devices is the fact that the spin relaxation time in a semiconducting media is short disabling the spin transport and then resulting in a no observable spin current.[9] In PSCs there is no net motion of charge; spin-up electrons move in a given direction while spin-down electrons travel in the opposite one. This phenomena can result from spin injection,[10] Hall Effects,[11] interference of two optical beams,[12,13] or one photon absorption of linearly polarized light[14] and has been observed in gallium arsenide (GaAs),[15,16] aluminum-gallium arsenide (AlGaAs),[16] and $Co_2FeSi$.[17]

Graphene, an allotrope of carbon with hexagonal 2D lattice structure presents properties like fractional quantum Hall effect at room temperature, excellent thermal transport properties, excellent conductivity[18] and strength[19–22] being then a perfect platform to be used in two-dimensions electronic systems; however most electronic applications are disabled by the absence of a semiconducting gap. Recent studies demonstrate that the band gap of graphene can be opened by applying an electric field,[23] reducing the surface area,[24] or applying uniaxial strain.[25] Another possibility to open the gap is by doping; this has been successfully achieved using nitrogen,[26] boron-nitrogen,[27] silicon,[28] noble-metals,[29] and hydrogen.[30–32] Depending on the percentage of hydrogenation and spatial configurations of hydrogen-carbon bonds, hydrogenated graphene can result in different spatial configurations. In this paper we present two 50% hydrogenated graphene noncentrosymmetric structures both presenting a discernible band gap: the *up* structure, shown in Fig. 1, has hydrogen atoms bonded to the carbon layer only in the upper side of the structure while the *alt* structure, shown in Fig. 2, has hydrogen alternating in the upper and bottom sides of the carbon slab.[33]

Using those structures we address a theoretical study of the spin velocity injection (SVI) by one-photon absorption of linearly polarized light. Because we have 2D structures we made the analysis for tow cases. The first is fixing the spin of the electrons along the $z$ Cartesian direction with the velocity directed on the surface of the structure in the $xy$ plane. The second is fixing the spin velocity in the $x$ or $y$ direction and the spin directed in $xyz$. The SVI is an optical effect that quantifies the velocity at which a PSC moves along the Cartesian direction a with the spin of electron polarized along the Cartesian direction b. One photon absorption of linearly polarized light can promote a distribution of electrons in $\mathbf{k}$ space regardless the symmetry of the material resulting in a null electrical current. Then, the electrons excited to the conduction bands at opposite $\mathbf{k}$ points will result in opposite spin polarizations producing no net spin injection.[14] If the crystalline structure of the material is noncentrosymmetric the spin polarization injected at a given $\mathbf{k}$ point could not vanish[34,35] and then, since the velocities of electrons at opposite $\mathbf{k}$ points are opposite, a pure spin current will be produced. Since the structures presented here are noncentrosymmetric, they are good candidates in which this effect can be induced.

This paper is organized as follows. In Section II we present the theory and formulas that describe PSC and SVI. In Section III we describe the details of calculations and the corresponding SVI spectra for the *up* and *alt* structures. Finally, we present our conclusions in Section IV.

## II. THEORY

In this section, we report a summary of the theory that involves the PSC phenomena from which rises the SVI treated in this paper.

In PSCs there is no net motion of electrical charge and spin-up electrons move in a given direction while spin-down electrons travel in the opposite one. This effect can result from one photon absorption of linearly polarized light by a semiconductor, with filled valence bands and empty conduction bands, illuminated by light with photon energy larger than the energy gap. Using a single continuous linearly polarized laser beam, it is possible to promote electrons in $\mathbf{k}$ space regardless the symmetry of the system re-

sulting in a net current equal to zero. If the phenomena is produced in a noncentrosymmetric semiconducting media, the electrons promoted to the conduction bands at opposite $\mathbf{k}$ points can produce a net spin polarization different to zero[34], resulting in a PSC because the velocity of electrons at opposite $\mathbf{k}$ points are in opposite directions.

Using the multiple scale approach to solve the equation of motion for the single particle density matrix $\rho_{mn}(\mathbf{k};t)$ we have that

$$\frac{\partial \rho_{cc'}}{\partial t} = -i(\omega_{cc'} - i\epsilon)\rho_{cc'} + \frac{e^2 E^{\mathrm{a}}(\omega)E^{\mathrm{b}*}(\omega)}{i\hbar^2}\times \sum_v r^{\mathrm{a}}_{cv} r^{\mathrm{b}}_{vc'} \left(\frac{1}{\omega - \omega_{c'v} - i\epsilon} - \frac{1}{\omega - \omega_{cv} + i\epsilon}\right).$$

Taking in the first term $\epsilon \to 0$ and changing the density matrix operator to the interaction representation, $\tilde{\hat{\rho}} = e^{iH_0 t/\hbar}\hat{\rho}e^{-iH_0 t/\hbar}$, with $H_0$ the ground state Hamiltonian, the matrix elements can be written as

$$\tilde{\rho}_{cc'(\mathbf{k})} = \langle c\mathbf{k}|\tilde{\hat{\rho}}|c'\mathbf{k}\rangle = e^{i\omega_{cc'}t}\rho_{cc'}(\mathbf{k}).$$

where $H_0|n\mathbf{k}\rangle = \hbar\omega_n(\mathbf{k})|n\mathbf{k}\rangle$ with $\hbar\omega_n(\mathbf{k})$ the energy of the electronic band $n$ at point $\mathbf{k}$ in the irreducible Brillouin zone (IBZ), and $|n\mathbf{k}\rangle$ the Bloch state. Then, the time derivative of $\tilde{\rho}_{cc'}(\mathbf{k})$ is given by

$$\frac{d\tilde{\rho}_{cc'}(\mathbf{k})}{dt} = \frac{e^2 E^{\mathrm{a}}(\omega)E^{\mathrm{b}*}(\omega)}{i\hbar^2}e^{i\omega_{cc'}t}\times \sum_v r^{\mathrm{a}}_{cv} r^{\mathrm{b}}_{vc'} \left(\frac{1}{\omega - \omega_{c'v} - i\epsilon} - \frac{1}{\omega - \omega_{cv} + i\epsilon}\right), \tag{1}$$

where $\epsilon \to 0$ still needs to be taken. The expectation value of an observable $\mathcal{O}$ with quantum mechanical operator associated $\hat{\mathcal{O}}$ is given by

$$\mathcal{O} = \mathrm{Tr}(\hat{\rho}\hat{\mathcal{O}}), \tag{2}$$

where Tr denotes the trace. Then

$$\mathcal{O} = \int \frac{d^3k}{8\pi^3}\sum_c \langle c\mathbf{k}|\hat{\rho}\hat{\mathcal{O}}|c\mathbf{k}\rangle = \int \frac{d^3k}{8\pi^3}\sum_{cc'} \tilde{\rho}_{cc'}(\mathbf{k})\mathcal{O}_{c'c}(\mathbf{k}), \tag{3}$$

where we used the interaction picture representation, $\tilde{\mathcal{O}}_{cc'} = \langle c'\mathbf{k}|e^{iH_0 t/\hbar}\hat{\mathcal{O}}e^{-iH_0 t/\hbar}|c\mathbf{k}\rangle$, and the closure relationship $\sum_c |c\mathbf{k}\rangle\langle c\mathbf{k} = 1$. So, the rate of change of $\mathcal{O}$ can be written from Eq. (1), Eq. (2), and Eq. (3) as

$$\dot{\mathcal{O}} = \mathrm{Tr}\left(\frac{d\hat{\tilde{\rho}}}{dt}\tilde{\mathcal{O}}\right), = \frac{e^2}{i\hbar^2}\int \frac{d^3k}{8\pi^3}\sum \mathcal{O}_{c'c} r^{\mathrm{a}}_{cv} r^{\mathrm{b}}_{vc'}\times \left(\frac{1}{\omega - \omega_{c'v} - i\epsilon} - \frac{1}{\omega - \omega_{cv} + i\epsilon}\right) E^{\mathrm{a}}(\omega)E^{\mathrm{b}*}(\omega) \tag{4}$$

Replacing the operator $\mathcal{O} \to \hat{K}^{\mathrm{ab}} \equiv v^{\mathrm{a}}S^{\mathrm{b}}$ the matrix elements are given by

$$K^{\mathrm{ab}}_{nm}(\mathbf{k}) = \sum_l v^{\mathrm{a}}_{nl}(\mathbf{k})S^{\mathrm{b}}_{lm}(\mathbf{k}), \tag{5}$$

and using time-reversal invariance it follows that

$$K^{\mathrm{ab}}_{nm}(-\mathbf{k}) = K^{\mathrm{ab}*}_{nm}(\mathbf{k}). \tag{6}$$

Now the time derivative $\dot{K}^{\mathrm{ab}}$ can be obtained as we proceeded in Eq. (A1) of Appendix A and then we write

$$\dot{K}^{\mathrm{ab}}(\omega) = \mu^{\mathrm{abcd}}(\omega)E^{\mathrm{c}}(\omega)E^{\mathrm{d}*}(\omega), \tag{7}$$

where the pure spin-current pseudotensor components

$$\mu^{\mathrm{abcd}}(\omega) = \frac{\pi e^2}{\hbar^2}\int \frac{d^3K}{8\pi^3}\times \sum_{vcc'}{}' \mathrm{Re}\left[K^{\mathrm{ab}}_{cc'}\left(r^{\mathrm{c}}_{vc'}r^{\mathrm{d}}_{cv} + (c \leftrightarrow d)\right)\right]\delta(\omega - \omega_{cv}), \tag{8}$$

are obtained from Eq. (A3) of the Appendix. The $'$ in the sum means that $c$ and $c'$ are quasi degenerate states and the sum only covers these states and since $\mu^{\mathrm{abcd}}(\omega)$ is real we have that $\mu^{\mathrm{abcd}}(\omega) = \mu^{\mathrm{abdc}}(\omega)$. This previous equation is the same as Eq. (3) of Bhat et al.[14] obtained by using the semiconductor optical Bloch equations.

### A. Spin velocity injection

We define the SVI as the velocity at which the spin, polarized along the direction a, propagates

along the direction b as

$$\mathcal{V}^{\mathrm{ab}}(\omega) \equiv \frac{\dot{K}^{\mathrm{ab}}(\omega)}{(\hbar/2)\dot{n}(\omega)}, \tag{9}$$

where $\dot{K}^{\mathrm{ab}}(\omega)$ is given by Eqns. (7) and (8) and the carrier injection rate, $\dot{n}(\omega)$, are given by

$$\dot{n}(\omega) = \xi^{\mathrm{ab}}(\omega) E^{c}(\omega) E^{d*}(\omega), \tag{10}$$

where $\xi^{\mathrm{ab}}(\omega)$ are the carrier generation rate tensor components. Since we have 2D structures we use an incoming electric field parallel to the surface, $\mathbf{E}^{\mathrm{a}}(\omega,\alpha) = E^{\mathrm{a}}(\omega)e^{i\alpha}$, where $\alpha$ corresponds to the linear polarization angle. Then from Eq. (7), Eq. (9), and (10), and including the polarization angle dependence we obtain

$$\mathcal{V}^{\mathrm{ab}}(\omega,\alpha) = \frac{2}{\hbar}\frac{\mu^{\mathrm{abxx}}(\omega)\cos^2(\alpha) + \mu^{\mathrm{abyy}}(\omega)\sin^2(\alpha) + \mu^{\mathrm{abxy}}(\omega)\sin(2\alpha)}{\xi^{\mathrm{xx}}(\omega)\cos^2(\alpha) + \xi^{\mathrm{yy}}(\omega)\sin^2(\alpha)}, \tag{11}$$

Two interesting possibilities to analyze the SVI are fixing the spin along $z$, directed perpendicularly to the surface of the structure, or fixing the velocity along $x$ or $y$ on the $xy$ plane of the structures. Also we can analyze the SVI contribution coming from each layer of the structure. In following subsections we present these three cases.

### B. Fixing spin

Analyzing the SVI, Eq. (11), we define the magnitude of the spin velocity with spin polarized along the b direction as

$$|\mathcal{V}_{\sigma^{\mathrm{b}}}(\omega,\alpha)| = \sqrt{[\mathcal{V}^{\mathrm{xb}}(\omega,\alpha)]^2 + [\mathcal{V}^{\mathrm{yb}}(\omega,\alpha)]^2}\,, \tag{12}$$

and the angle at which the spin velocity is directed on the $xy$ plane as

$$\gamma_{\mathrm{b}}(\omega,\alpha) = \tan^{-1}\left(\frac{\mathcal{V}^{\mathrm{yb}}(\omega,\alpha)}{\mathcal{V}^{\mathrm{xb}}(\omega,\alpha)}\right), \tag{13}$$

where this angle is measured in the counterclockwise direction from the positive $x$. We also define two special angles

$$\gamma_{\mathrm{b}\parallel}(\omega,\alpha) = \alpha, \tag{14}$$

and

$$\gamma_{\mathrm{b}\perp}(\omega,\alpha) = \alpha \pm 90^{\circ}. \tag{15}$$

The first corresponds to the case when the spin velocity is directed, in the same direction of the polarization angle $\alpha$ of the incoming beam and the second one corresponds to the case when the spin velocity is directed perpendicularly with respect to the polarization angle of the incoming beam.

### C. Fixing velocity.

Fixing the velocity along $x$ or $y$ we define the corresponding magnitude as

$$|\mathcal{V}^{\mathrm{a}}(\omega,\alpha)| = \sqrt{[\mathcal{V}^{\mathrm{ax}}(\omega,\alpha)]^2 + [\mathcal{V}^{\mathrm{ay}}(\omega,\alpha)]^2 + [\mathcal{V}^{\mathrm{az}}(\omega,\alpha)]^2}., \tag{16}$$

Then, the spin direction depends on the components of the previous equation and so we define the spin orientation polar and azimuthal angles as

$$\theta_{\mathrm{a}}(\omega,\alpha) = \cos^{-1}\left(\frac{\mathcal{V}^{\mathrm{az}}(\omega,\alpha)}{|\mathcal{V}^{\mathrm{a}}(\omega,\alpha)|}\right), \quad 0 \leq \theta \leq \pi, \tag{17}$$

$$\varphi_{\mathrm{a}}(\omega,\alpha) = \tan^{-1}\left(\frac{\mathcal{V}^{\mathrm{ay}}(\omega,\alpha)}{\mathcal{V}^{\mathrm{ax}}(\omega,\alpha)}\right), \quad 0 \leq \varphi \leq 2\pi. \tag{18}$$

### D. Layer-by-layer analysis.

For a layered system we have that the total contribution of Eqns. (12) and (16) are given[36]

| Layer No. | Atom type | Position [Å] $x$ | $y$ | $z$ |
|---|---|---|---|---|
| 1 | H | -0.61516 | -1.77416 | 0.73196 |
| 1 | H | 0.61518 | 0.35514 | 0.73175 |
| 2 | C | -0.61516 | -1.77264 | -0.49138 |
| 2 | C | -0.61516 | -0.35600 | -0.72316 |
| 2 | C | 0.61516 | 0.35763 | -0.49087 |

TABLE I. Unit cell of *up* structure. Layer division, atom types and positions for the *up* structure. The structure unit cell was divided in two layers corresponding to hydrogen and carbon atoms.The corresponding layer atom position is depicted in Fig. 1 with the corresponding number of layer.

| Layer No. | Atom type | Position [Å] $x$ | $y$ | $z$ |
|---|---|---|---|---|
| 1 | H | -0.61516 | -1.42140 | 1.47237 |
| 2 | C | -0.61516 | -1.73300 | 0.39631 |
| 3 | C | 0.61516 | 1.73300 | 0.15807 |
| 4 | C | 0.61516 | 0.42201 | -0.15814 |
| 5 | C | -0.61516 | -0.37396 | -0.39632 |
| 6 | H | -0.61516 | -0.68566 | -1.47237 |

TABLE II. Unit cell of *alt* structure. Layer division, atom types and positions for the *alt* structure. The structure unit cell was divided in six layers corresponding each one to atoms in different $z$ positions. The corresponding layer atom position is depicted in Fig. 2 with the corresponding number of layer.

by

$$|\mathcal{V}_{\sigma^{\rm b}}(\omega,\alpha)| = \sum_{\ell=1}^{N_{\rm eff}} |\mathcal{V}_{\sigma^{\rm b}}(\ell|\omega,\alpha)| \qquad (19)$$

$$|\mathcal{V}^{\rm a}(\omega,\alpha)| = \sum_{\ell=1}^{N_{\rm eff}} |\mathcal{V}^{\rm a}(\ell|\omega,\alpha)| \qquad (20)$$

where $|\mathcal{V}_{\sigma^{\rm b}}(\ell|\omega,\alpha)|$ and $|\mathcal{V}^{\rm a}(\ell|\omega,\alpha)|$ gives the contribution of the $\ell^{th}$ layer to the total SVI when the spin is fixed in the b direction or when the velocity is fixed in the a direction, respectively. For the structures presented here this layers correspond to the total number of layers being two for the *up* structure and six for the *alt* structure.

## III. RESULTS

We preset the results for $|\mathcal{V}^{\rm a}(\omega,\alpha)|$ and $|\mathcal{V}_{\sigma^{\rm b}}(\omega,\alpha)|$ for the $C_{16}H_8$-alt and $C_{16}H_8$-up structures being both noncentrosymmetric semi-infinite 2D carbon systems with 50% hydrogenation in different arrangements. We recall that the *up* structure has hydrogen atoms only on the upper side of the carbon sheet while the *alt* structure has alternating hydrogen atoms on the upper and bottom sides. Also we take the hexagonal carbon lattice to be on the $xy$ plane for both structures, and the carbon-hydrogen bonds on the perpendicular $xz$ plane, as depicted in Figs. 2 and 1. The coordinates for the *up* and *alt* unit cells of the structures are presented in Tables I and II.

We calculated the self-consistent ground state and the Kohn-Sham states using density functional theory in the local density approximation (DFT- LDA) with a planewave basis using the ABINIT code[37]. We used Hartwigsen-Goedecker-Hutter (HGH) relativistic separable dual-space Gaussian pseudopotentials[38] including the spin-orbit interaction needed to calculate $\mu^{\rm abcd}(\omega,\alpha)$ presented in Eq. (8). The convergence parameters for the calculations of our results corresponding to the *alt* and *up* structures are cutoff energies of 65 Ha and 40 Ha, resulting in LDA energy band gaps of 0.72 eV and 0.088 eV, respectively. The energy eigenvalues and matrix elements for the *up* and *alt* structures were calculated using 14452 **k** points and 8452 **k** points in the IBZ. It is known that the DFT with LDA approximation misestimates the energy band gap of semiconductors. To correct this one has to include the many-body interaction using i.e. the so-called GW approximation but this technique has a very high computational cost and is out of the scope in this paper. Nevertheless, DFT still remains a mainstream tool for calculating diverse properties derived from the electronic band structure.

### A. Spin velocity injection

Using the Eq. (11), we calculated the $\mathcal{V}^{\rm ab}(\omega,\alpha)$ response for the *up* and *alt* 2D struc-

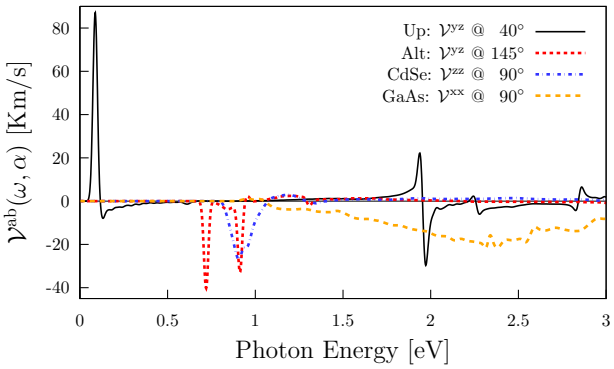


FIG. 3. Comparison of most intense responses of $\mathcal{V}^{ab}$ for 2D *alt* and *up*, and bulk CdSe and GaAs structures and their corresponding polarization angle $\alpha$.

tures and for the CdSe and GaAs bulk systems; the results are presented in Fig. 3. The angle $\alpha$ presented in the response of each structure is that for which the response is maximized in each case. The most intense response corresponds to the *up* structure centered at 0.088 eV corresponding to the Mid Infrared (MIR) radiation and reaching a spin velocity of 87.2 Km/s. For an energy range from 0.66 eV to 3.0 eV, corresponding to energies of the Near Infrared (NIR) to visible radiation, all the four structures have contributions of the same order of magnitude. For this energy range the *up* structure has two peaks centered at 1.94 eV and 1.97 eV reaching spin velocities of 22.2 Km/s and -29.7 Km/s and the *alt* structure has two peaks centered at 0.72 eV and 0.91 eV reaching spin velocities of -40.2 Km/s and -32.9 Km/s, respectively. Then, for the bulk structures we have that the CdSe has only one intense response centered at 0.91 eV reaching a spin velocity of -26.9 Km/s, and the GaAs structure response reaches the maximum for an incoming beam of energy of 2.31 eV and resulting in a spin velocity of -21.6 Km/s. In table III we present the comparison of this values for the 2D and bulk structures; a positive (negative) spin-velocity means that the velocity moves (anti-)parallel to the electric field. From the table also we obtain that particularly the 2D *up* structure is the one with the highest response being between 4 and 5 times more intense than the corresponding to the bulk structures.

| Structure | Kind of system | Pol. Ang. | Energy [eV] | $\mathcal{V}^{ab}(\omega,\alpha)$ ab | [Km/s] |
|---|---|---|---|---|---|
| *up* | 2D | 40 | 0.09 | yz | 87.2 |
| | | | 1.94 | yz | 22.2 |
| | | | 1.97 | yz | -29.7 |
| *alt* | 2D | 145 | 0.72 | yz | -40.2 |
| | | | 0.91 | yz | -32.9 |
| CdSe | bulk | 90 | 0.91 | zz | -26.9 |
| GaAs | bulk | 90 | 2.31 | xx | -21.6 |

TABLE III. Comparison of the reported maxima values of $\mathcal{V}^{ab}$ for the different structures and their corresponding polarization angle $\alpha$ and energy values of the incoming beam at which the maxima is obtained.

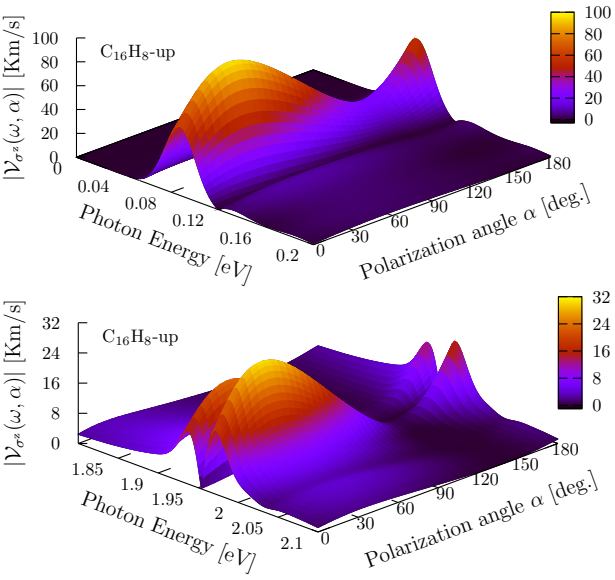


FIG. 4. $|\mathcal{V}_{\sigma^z}(\omega,\alpha)|$ response as a function of the photon energy and polarization angle $\alpha$ for the *up* structure for two energy ranges. The absolute maxima is located for an energy range from 0.08 eV to 0.10 eV, in the Far Infrared radiation range, and two local maxima from 1.90 eV to 1.93 eV and from 1.96 eV to 2.0 eV, in the visible radiation range, all for polarization angles between 25° and 50°.

### B. Fixing spin

Using Eq. (12), we calculated $|\mathcal{V}_{\sigma^b}(\omega,\alpha)|$ and made the analysis for the case when the spin is fixed along $z$ directed perpendicularly to the surface of the *up* and *alt* structures. Also, using Eq. (13), we determined the angle $\gamma_b(\omega,\alpha)$ where the spin-velocity is directed on the surface of the each structure.

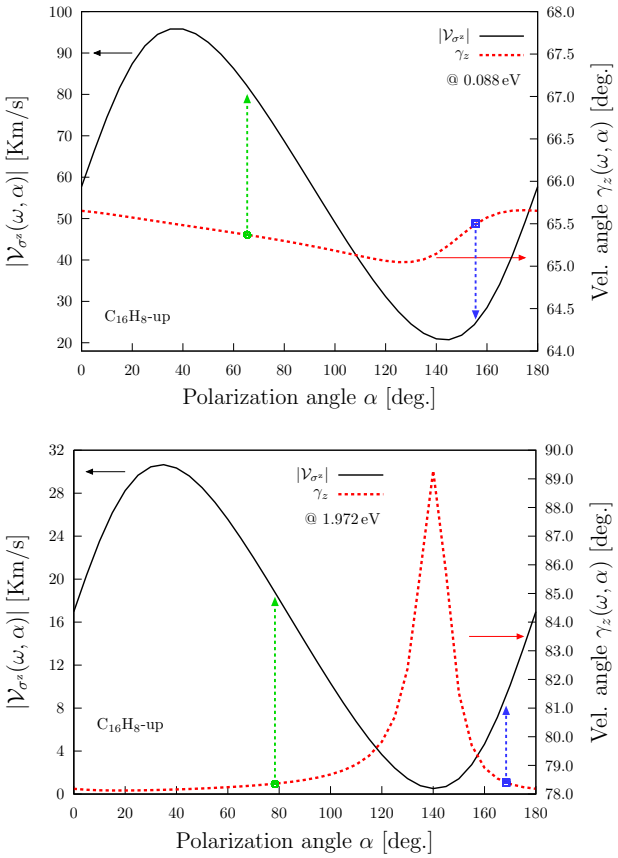


FIG. 5. Most intense response of $|\mathcal{V}_{\sigma^z}(\omega,\alpha)|$ (top frames, right scale of figs (a) and (b)), the corresponding velocity angle $\gamma_z(\omega,\alpha)$ (top frames, right scale), the collinear (circled box) and perpendicular (square box) angles, and the two components $\mathcal{V}^{xz}(\omega,\alpha)$ and $\mathcal{V}^{yz}(\omega,\alpha)$ (bottom frames) for the *up* structure fixing the energy to 0.088 eV.

### 1. *Up structure*

We present in Fig. 4 the result of evaluate $|\mathcal{V}_{\sigma^z}(\omega,\alpha)|$ (Eq. (12)) for two energy ranges on the *up* structure. We obtained that the zone where the maximum response is reached corresponds to a energy range of the incident beam from 0.084 eV to 0.093 eV, in the far infrared (FIR) and polarization angles $\alpha$ between 30° and 45°. Also the two local maxima are held for same beam polarization angles but for an energy range between 1.90 eV and 2.05 eV, in the visible radiation range. In the top panel of Fig. 5 we present the result of evaluate Eq. (12) (left scale, black solid line) fixing the energy of the incoming beam to 0.088 eV for which the response is maximized as shown in the top panel of Fig. 4. The absolute maximum is obtained when the polarization angle is $\alpha = 40°$ resulting in a value of $|\mathcal{V}_{\sigma^z}(\omega,\alpha)| = 95.8$ Km/s. This value comes from the contribution of the components $\mathcal{V}^{xz}(\omega,\alpha) = 39.8$ Km/s and $\mathcal{V}^{yz}(\omega,\alpha) = 87.2$ Km/s not presented here. In the same panel we present the corresponding velocity angle $\gamma_z(\omega,\alpha)$ (right scale, red dashed line), that for the absolute maximum is $\gamma_z(\omega,\alpha) = 65°$. Also we present two boxes indicating the values for which the angles of the spin velocity and the polarization angle are parallel (Eq. 14, green circled box), corresponding to $\alpha = \gamma_{z\|}(\omega,\alpha) = 65.5°$; and perpendicular (Eq. 15, blue squared box), corresponding to $\alpha = 155.5°$ and $\gamma_{z\perp}(\omega,\alpha) = 65.5°$. The green and blue dashed arrows are directed from those angles to the respective value of the response corresponding to $|\mathcal{V}_{\sigma^z}(\omega,\alpha)| = 82.3$ Km/s and $|\mathcal{V}_{\sigma^z}(\omega,\alpha)| = 24.8$ Km/s. We also found that the velocity angle is almost constant for all the polarization angle range having values of $\gamma_z(\omega,\alpha) = 65.5° \pm 0.5°$. In the bottom panel of Fig. 5 we present for the same structure the result of evaluate Eq. (12) fixing now the energy of the incoming beam to 1.972 eV for which the response has a local maximum as shown in the bottom panel of Fig. 4. The local maximum is obtained again when the polarization angle is $\alpha = 40°$ resulting in a value of $|\mathcal{V}_{\sigma^z}(\omega,\alpha)| = 30.3$ Km/s directed in a velocity angle $\gamma_z(\omega,\alpha) = 78°$. Again, the green circled box indicates the parallel angles $\alpha = \gamma_{z\|}(\omega,\alpha) = 78.5°$ corresponding to a spin-velocity $|\mathcal{V}_{\sigma^z}(\omega,\alpha)| = 23.5$ Km/s indicated with the green arrow and the blue squared box indicates the perpendicular pair of angles $\alpha = 155.5°$ and $\gamma_{z\perp}(\omega,\alpha) = 65.5°$. We found again that the velocity angle is almost constant at 78° and has variations of $\pm 1°$ for polarization angles $0° \leq \alpha \leq 100°$. We also made the analysis for the cases when the spin polarization is directed along x and y but we do not present here the corresponding plots. For those cases we have that the responses maxima are obtained for an energy of 0.088 eV and polarization angle $\alpha = 40°$ resulting in values of $|\mathcal{V}_{\sigma^x}(\omega,\alpha)| = 37.4$ Km/s and $|\mathcal{V}_{\sigma^y}(\omega,\alpha)| = 24.8$ Km/s.

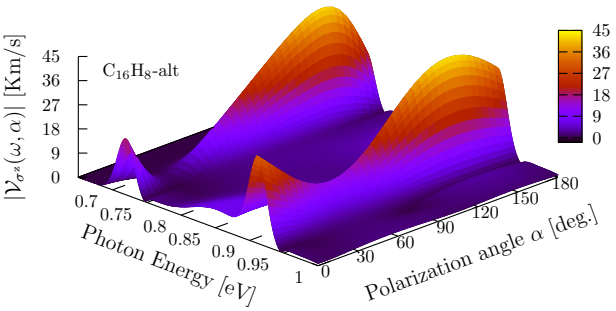


FIG. 6. $|\mathcal{V}_{\sigma^z}(\omega,\alpha)|$ response as a function of the photon energy and polarization angle $\alpha$ for the *alt* structure. The local and the absolute maxima are located in the energy ranges from 0.67 eV to 0.73 eV and from 0.90 eV to 0.93 eV, respectively, and both in the Near Infrared and for polarization angles between 120° and 150°.

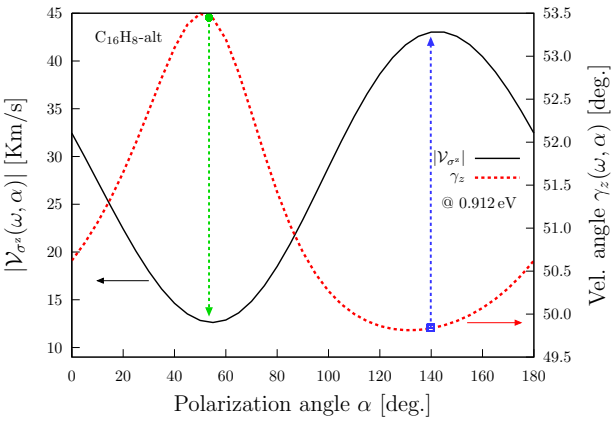


FIG. 7. Most intense response of $|\mathcal{V}_{\sigma^z}(\omega,\alpha)|$ (top frame, left scale) the corresponding velocity angle $\gamma_z(\omega)$ (top frame, right scale), the collinear (circled box) and perpendicular (square box) angles, and the two components $\mathcal{V}^{xz}(\omega)$ and $\mathcal{V}^{yz}(\omega)$ (bottom frame) for the *alt* structure fixing the energy to 0.912 eV.

### 2. *Alt structure*

We present in Fig. 6 the result of evaluate $|\mathcal{V}_{\sigma^z}(\omega,\alpha)|$ (Eq. (12)) on the *alt* structure. We obtained that the zone where the maximum response is reached corresponds to energies from 0.90 eV to 0.93 eV and a local maximum is obtained for energies between 0.67 eV and 0.75 eV both located in the FIR radiation range and for polarization angles between 120° and 150°. In the top panel of Fig. 5 we present the result of evaluate Eq. (12) (left scale, black solid line) fixing the energy to 0.912 eV for which the response is maximized as shown in the top panel of Fig. 4. The absolute maximum is obtained when the polarization angle is $\alpha = 40°$ resulting in a value of $|\mathcal{V}_{\sigma^z}(\omega,\alpha)| = 43.0$ Km/s. In the same panel we present the velocity angle $\gamma_z(\omega,\alpha)$ (right scale, red dashed line), that for the absolute maximum is $\gamma_z(\omega,\alpha) = 145°$. As explained for the previous case, the green circled box indicates the parallel pair of angles $\alpha = \gamma_{z\parallel}(\omega,\alpha) = 53.5°$ with a corresponding value $|\mathcal{V}_{\sigma^z}(\omega,\alpha)| = 12.7$ Km/s indicated with the green arrow, and the blue square box indicates the perpendicular pair of angles, $\alpha = 140°$ and $\gamma_{z\perp}(\omega,\alpha) = 50°$, with a value of $|\mathcal{V}_{\sigma^z}(\omega,\alpha)| = 43.0$ Km/s indicated with the blue arrow. We also have that the velocity angle is centered at 51.5° having variations of ±2° for the polarization angle range $0° \leq \alpha \leq 180°$. Again, for the cases in which the spin polarization is parallel to the surface of the *alt* structure was calculated but the plots are not presented here. The absolute maxima for the cases when the spin polarization are directed in the $x$ and $y$ direction are obtained for an energy of 0.912 eV and polarization angle $\alpha = 145°$ resulting in values of $|\mathcal{V}_{\sigma^x}(\omega,\alpha)| = 27.1$ Km/s and $|\mathcal{V}_{\sigma^y}(\omega,\alpha)| = 33.2$ Km/s.

## C. Fixing velocity

Now, using the Eq. (16), we calculated the $|\mathcal{V}^a(\omega,\alpha)|$ for the case when the velocity is fixed in the $x$ and $y$ direction on the surface of the *up* and *alt* structures. Also, using the Eqns. (17) and (18), we determined the polar $\theta_a(\omega,\alpha)$ and azimuthal $\varphi_a(\omega,\alpha)$ angles corresponding to the direction of the spin.

### 1. *Up structure*

In top and bottom panels of Fig. 8 we present the result of evaluate Eq. (16) for the *up* structure fixing the velocity in the $x$ and $y$ direction. From this figure we can see that the two absolute maxima are obtained for energies between 0.084 eV and 0.093 eV, in the FIR, and polarization angles between 30° and 45°. In the top and bottom panels of Fig. 9 we present $|\mathcal{V}^x(\omega,\alpha)|$ and $|\mathcal{V}^y(\omega,\alpha)|$ (left scale, black solid

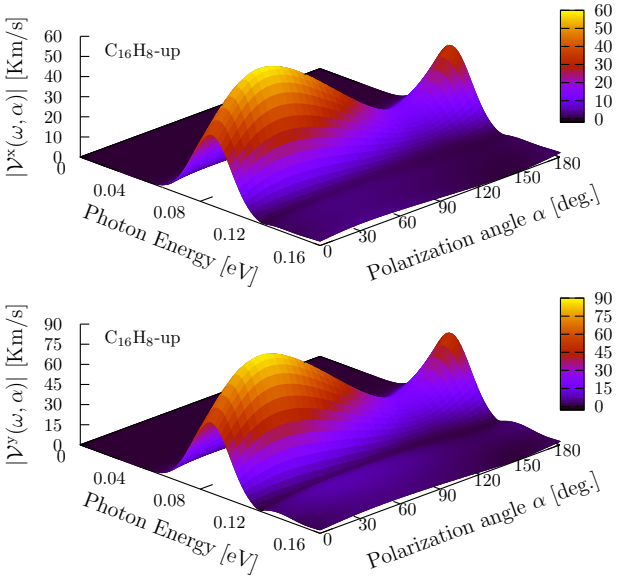


FIG. 8. $|\mathcal{V}^{\rm x}(\omega,\alpha)|$ and $|\mathcal{V}^{\rm y}(\omega,\alpha)|$responses as a function of the photon energy and polarization angle $\alpha$ for the *up* structure. The absolute maxima of both are localized in the energy range from 0.08 eV to 0.10 eV, in the Far Infrared, and for polarization angles from 25° to 50°.

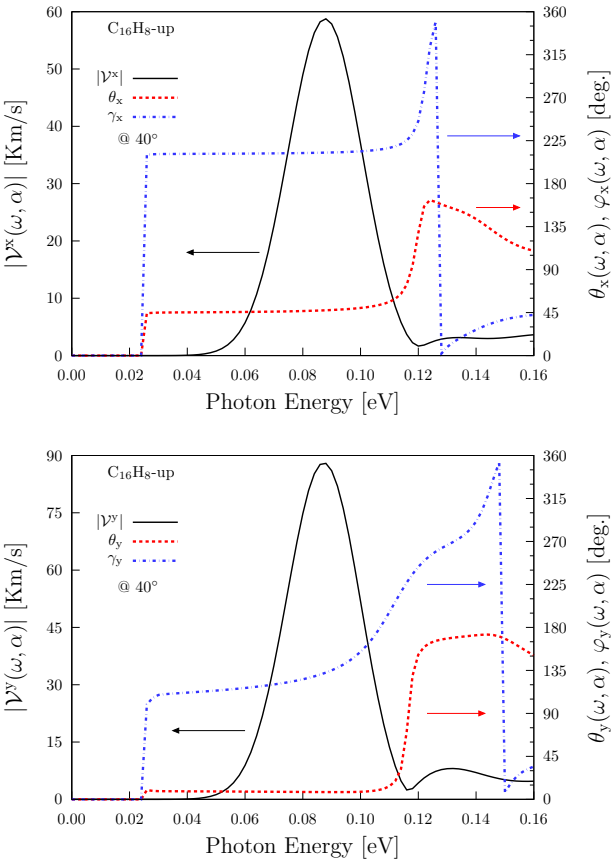


FIG. 9. Most intense response of $|\mathcal{V}^{\rm x}(\omega,\alpha)|$ and $|\mathcal{V}^{\rm y}(\omega,\alpha)|$ (top frames left scale of Figs. (a) and (b)), the corresponding polar $\varphi$ and azimuthal $\theta$ angles (top frames right scale), and the corresponding three components (bottom frames) for the *up* structure fixing the polarization angle to $\alpha = 40°$ to maximize the response.

line) fixing the polarization angle to $\alpha = 40°$ for which the responses have absolute maxima of 58.7 Km/s and 87.9 Km/s, respectively, for an energy of 0.088 eV. In same panels we present the corresponding polar (right scale, red dashed line) and azimuthal (right scale, blue dashed line) spin polarization angles that have values of $\theta_{\rm x}(\omega,\alpha) = 47°$, $\varphi_{\rm x}(\omega,\alpha) = 212°$, $\theta_{\rm y}(\omega,\alpha) = 8°$ and $\varphi_{\rm y}(\omega,\alpha) = 133°$. In this way, the spin is directed upward the third Cartesian quadrant of the $xy$ plane when it moves along $x$, and is directed almost perpendicularly over the $xy$ plane when it moves along $y$. Also from this figure we have that when the spin moves along $x$ the angles are almost constant for the peak of the response having variations of $\pm 2°$ but when the spin moves along $y$ the azimuthal angle changes from 99° to 176°

In top and bottom panels of Fig. 10 we present the result of evaluate Eq. (16) for the same structure fixing the velocity in the $x$ and $y$ direction for other range of energies that present a intense response. From this figure we can see that the two local maxima are obtained for energies between 1.80 eV and 2.10 eV, in the range of visible radiation, and polarization angles between 30° and 45°. From the top and bottom panels of Fig. 11 we have that $|\mathcal{V}^{\rm x}(\omega,\alpha)| = 9.8$ Km/s and $|\mathcal{V}^{\rm y}(\omega,\alpha)| = 49.3$ Km/s fixing the polarization angle to $\alpha = 40°$ and the beam energy to 1.932 eV. In same panels we present the corresponding polar and azimuthal spin polarization angles that have values of $\theta_{\rm x}(\omega,\alpha) = 129°$, $\varphi_{\rm x}(\omega,\alpha) = 229°$, $\theta_{\rm y}(\omega,\alpha) = 127°$ and $\varphi_{\rm y}(\omega,\alpha) = 227°$ being constant all of them in the peak of the local maxima. Then, the spin is directed downward the third Cartesian quadrant of the $xy$ plane when it moves along $x$ and $y$ directions.

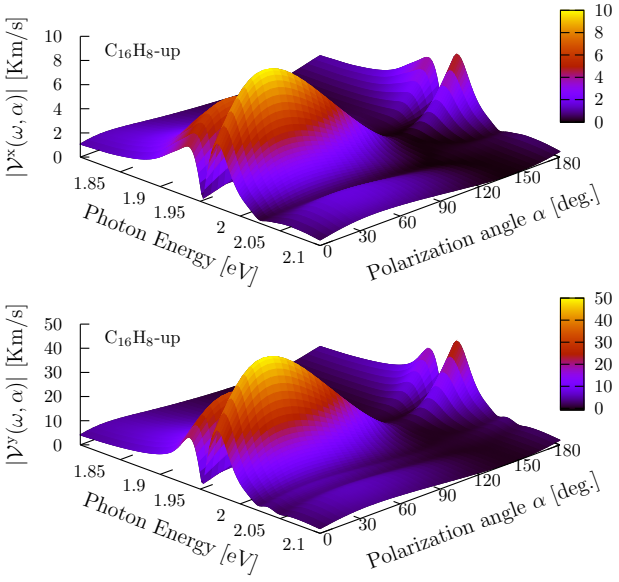


FIG. 10. $|\mathcal{V}^{\rm x}(\omega,\alpha)|$ (top panel) and $|\mathcal{V}^{\rm y}(\omega,\alpha)|$ (bottom panel) as a function of the photon energy and polarization angle $\alpha$ for the *up* structure. Two local maxima of both responses are localized in the energy range from 1.90 eV to 1.93 eV and from 1.96 eV to 2.0 eV, in the visible radiation range, and for polarization angles between 25° and 50°.

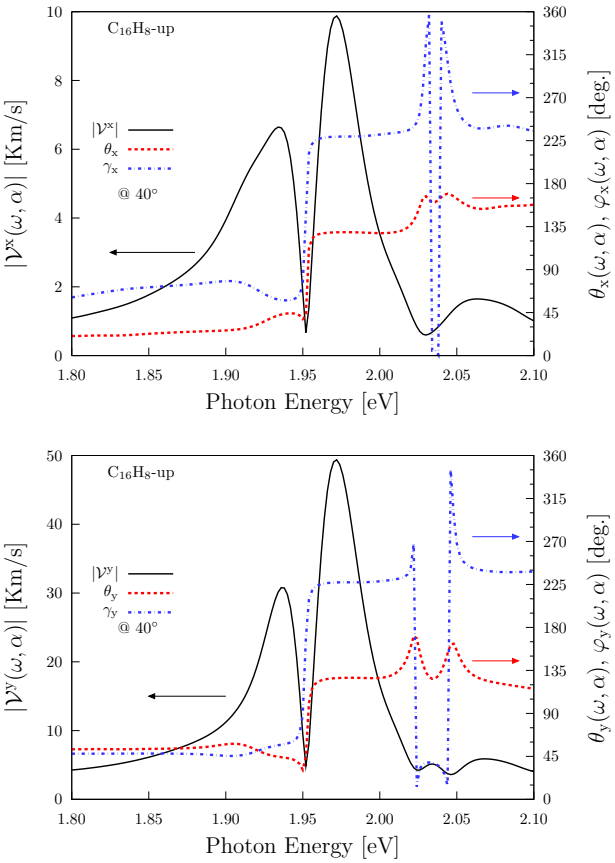


FIG. 11. Intense response of $|\mathcal{V}^{\rm x}(\omega,\alpha)|$ and $|\mathcal{V}^{\rm y}(\omega,\alpha)|$ (top frames left scale of Figs. (a) and (b)), the corresponding polar $\varphi$ and azimuthal $\theta$ angles (top frames right scale), and the corresponding three components (bottom frames) for the *up* structure fixing the polarization angle to $\alpha = 40°$ to maximize the response.

### 2. *Alt structure*

In top and bottom panels of Fig. 12 we present the result of evaluate Eq. (16) for the *up* structure fixing the velocity in the $x$ and $y$ direction. From this figure we have that the relative maxima for the spin velocity along $x$ and $y$ are obtained for energies between 0.70 eV to 0.75 eV and the absolute maxima are obtained for energies between 0.90 eV and 0.93 eV, all cases in the NIR radiation, and polarization angles between 120° and 150°. From the top and bottom panels of Fig. 13 we have that that the local maxima are $|\mathcal{V}^{\rm x}(\omega,\alpha)| = 19.4\,{\rm Km/s}$ and $|\mathcal{V}^{\rm y}(\omega,\alpha)| = 51.9\,{\rm Km/s}$ fixing the energy to 0.720 eV and the absolute maxima are $|\mathcal{V}^{\rm x}(\omega,\alpha)| = 30.9\,{\rm Km/s}$ and $|\mathcal{V}^{\rm y}(\omega,\alpha)| = 52.2\,{\rm Km/s}$ fixing the energy to 0.912 eV all for a polarization angle $\alpha = 145°$. The corresponding polar and azimuthal angles for the local maxima are $\theta_{\rm x}(\omega,\alpha) = 46°$, $\varphi_{\rm x}(\omega,\alpha) = 41°$, $\theta_{\rm y}(\omega,\alpha) = 141°$ and $\varphi_{\rm y}(\omega,\alpha) = 222°$ being the spin directed over the first Cartesian quadrant of the $xy$ plane when the spin velocity is directed along $x$ and directed downward the third Cartesian quadrant when the spin velocity is directed along $y$. Finally, the angles for the absolute maxima are $\theta_{\rm x}(\omega,\alpha) = 154°$, $\varphi_{\rm x}(\omega,\alpha) = 290°$, $\theta_{\rm y}(\omega,\alpha) = 129°$ and $\varphi_{\rm y}(\omega,\alpha) = 229°$ being the spin polarization directed downward the fourth Cartesian quadrant when the spin velocity is directed along $x$ and downward the third Cartesian quadrant when the spin velocity is directed along $y$.

## D. Layer-by-layer analysis

As mentioned before in in the beginning of this section the *up* and *alt* structures presented here was divided into layers to analyze the layer-by-layer contribution for $|\mathcal{V}_{\sigma^{\rm b}}(\omega,\alpha)|$ and

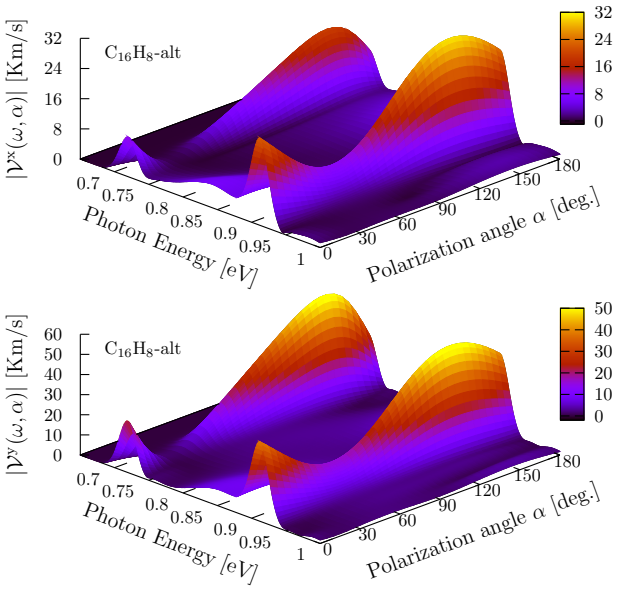


FIG. 12. $|\mathcal{V}^{x}(\omega,\alpha)|$ (top panel) and $|\mathcal{V}^{y}(\omega,\alpha)|$ (bottom panel) as a function of the photon energy and polarization angle $\alpha$ for the *alt* structure. The local and the absolute maxima are located in the energy ranges from 0.67 eV to 0.73 eV and from 0.90 eV to 0.93 eV, respectively, and both in the Near Infrared and for polarization angles between 120° and 150°.

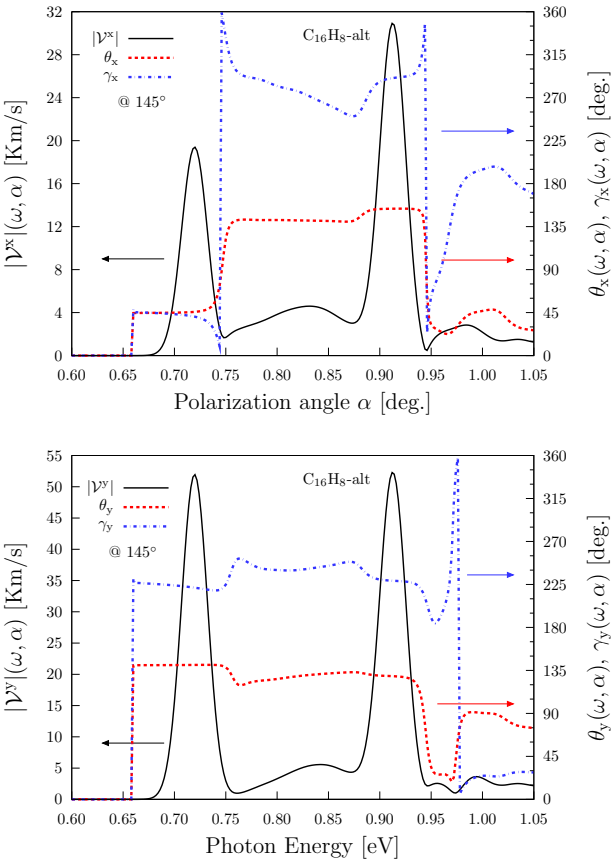


FIG. 13. Most intense response of $|\mathcal{V}^{x}(\omega,\alpha)|$ and $|\mathcal{V}^{y}(\omega,\alpha)|$ (top frames left scale of Figs. (a) and (b)), the corresponding polar $\varphi$ and azimuthal $\theta$ angles (top frames right scale), and the corresponding three components (bottom frames) for the *alt* structure fixing the polarization angle to $\alpha = 145°$ to maximize the response.

$|\mathcal{V}^{a}(\omega,\alpha)|$. In Tables I and II we present the layer division needed to calculate the layer-by-layer contribution for the $|\mathcal{V}_{\sigma^b}(\omega,\alpha)|$ and $|\mathcal{V}^{a}(\omega,\alpha)|$ presented in Eqns. (19) and (20). The *up* structure was divided in two layers, the first comprised of the top hydrogen atoms denoted by the number 1 in Table I and in the Fig. 1 and the second comprised of carbon atoms and denoted by the number 2. The *alt* structure was divided in six layers denoted with numbers from 1 to 6 in Table II and in Fig. 2. The first and sixth layers correspond to hydrogen atoms in the top and bottom positions and from the second to the fifth correspond to carbon atoms placed in different positions. Here we present the decomposition only for $|\mathcal{V}_{\sigma^z}(\omega,\alpha)|$ and for the corresponding components of the *up* structure in Figs. 14 and 15 and for the *alt* structure in Fig. 16.

From the central and bottom frames of Fig. 14 we have that when the energy is fixed to 0.088 eV almost all the response of the $\mathcal{V}^{xz}(\omega,\alpha)$ component comes from the second layer comprised by carbon atoms having a minimal reduction produced by the hydrogen layer. Also, the $\mathcal{V}^{yz}(\omega,\alpha)$ response, presented in bottom frame of same figure, is produced only by the carbon layer. This result in a total response $|\mathcal{V}_{\sigma^z}(\omega,\alpha)| = 95.8$ Km/s coming from the carbon layer and being minimally reduced by the hydrogen layer as shown in the top frame of this figure for a fixed polarization angle $\alpha = 40°$. Now, for the same structure but now fixing the energy to 1.972 eV we have from the central frame of Fig. 15 that the the carbon layer produces the response of the $\mathcal{V}^{zx}(\omega,\alpha)$ component being decreased by the hydrogen layer. Opposite to that, in the bottom frame of same figure we obtained that the response of the carbon and hydrogen layer are not inverse and then contributing both to the total response of $\mathcal{V}^{yz}(\omega,\alpha)$.

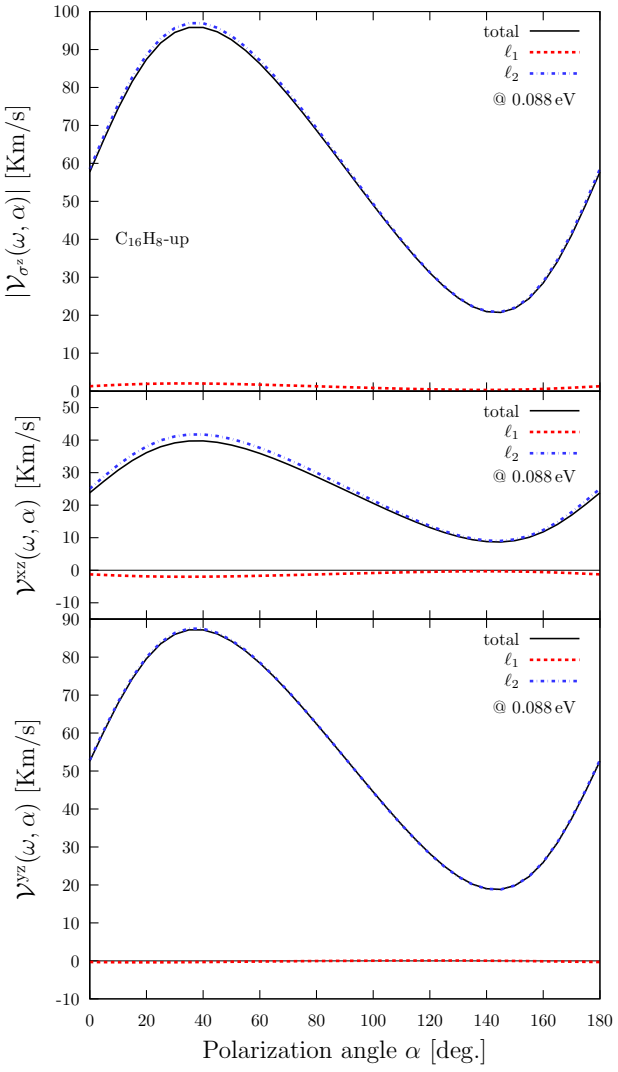


FIG. 14. Layer-by-layer contribution of the $|\mathcal{V}_{\sigma^z}(\omega,\alpha)|$ response (top frame) for the *up* structure as a function of the polarization angle $\alpha$ for the energy fixed to 0.088 eV for which the absolute maximum is obtained. The corresponding layered contributions for the $\mathcal{V}^{xz}(\omega,\alpha)$ and $\mathcal{V}^{zy}(\omega,\alpha)$ components are presented in the central and bottom frames.

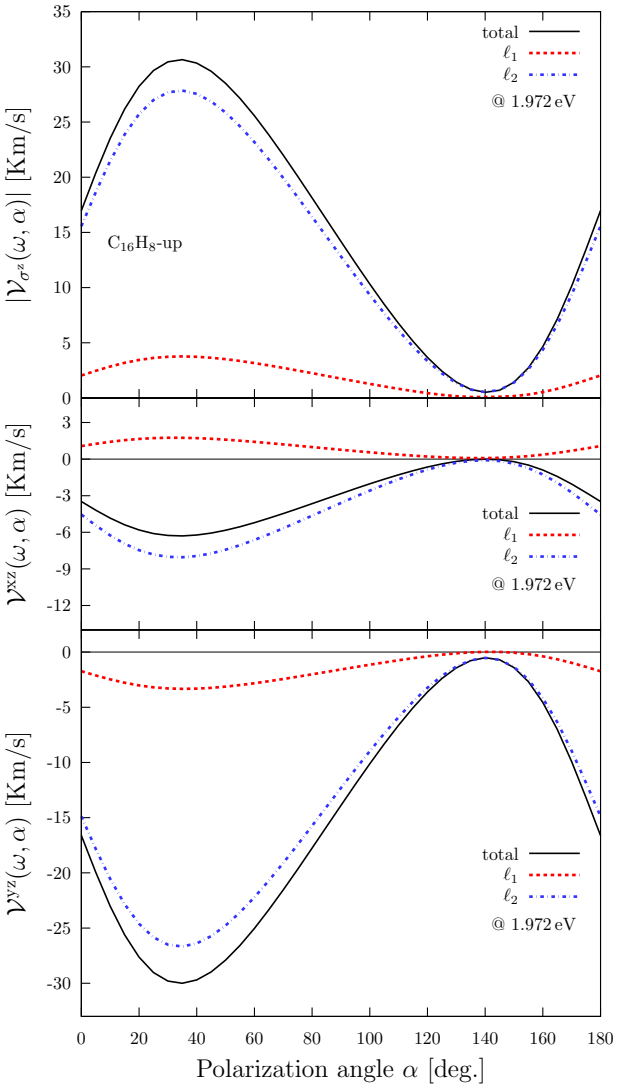


FIG. 15. Layer-by-layer contribution of the $|\mathcal{V}_{\sigma^z}(\omega,\alpha)|$ response (top frame) for the *up* structure as a function of the polarization angle $\alpha$ for the energy fixed to 1.972 eV for which a local maximum is obtained. The corresponding layered contributions for the $\mathcal{V}^{xz}(\omega,\alpha)$ and $\mathcal{V}^{zy}(\omega,\alpha)$ components are presented in the central and bottom frames.

Then, in the top frame of this figure we have that the major contribution to the $|\mathcal{V}_{\sigma^z}(\omega,\alpha)|$ response comes from the carbon layer with but being in this case reinforced by the contribution of the hydrogen layer and resulting in a value of 30.3 Km/s. Finally, for the *alt* structure we have that, for the response $|\mathcal{V}_{\sigma^z}(\omega,\alpha)|$ when the energy is fixed to 0.720 eV the six layers contribute with similar magnitudes. We found that for the $\mathcal{V}^{xz}(\omega,\alpha)$ and $\mathcal{V}^{yz}(\omega,\alpha)$ components the top hydrogen layer response, denoted by $\ell_1$, cancels partially the the bottom hydrogen layer response, denoted by $\ell_6$; a similar behavior occurs in the component $\mathcal{V}^{xz}(\omega,\alpha)$ for the third and fourth carbon layers and in the component $\mathcal{V}^{yz}(\omega,\alpha)$ for the second and fifth carbon layers. This result in a total response $\mathcal{V}^{xz}(\omega,\alpha) = 42.4$ Km/s for a fixed polarization angle $\alpha = 145°$. Then, for this analysis we found that the $|\mathcal{V}_{\sigma^z}(\omega,\alpha)|$ and in general, $\mu^{abcd}(\omega)$ responses are very susceptible to the symmetry

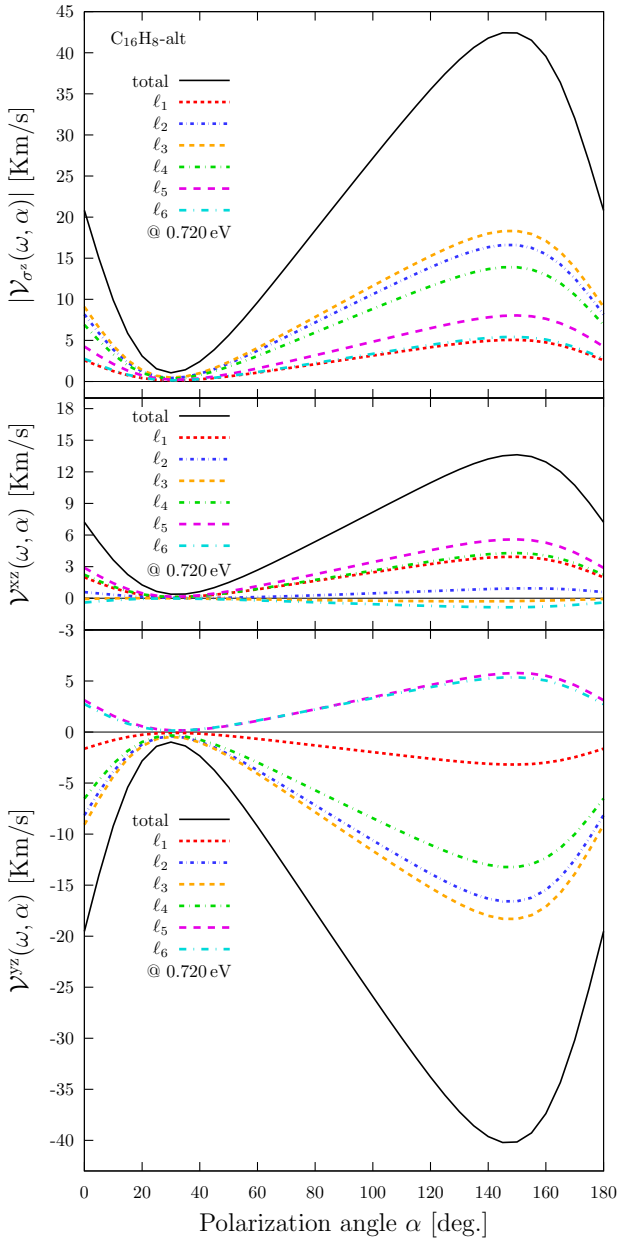


FIG. 16. Layer-by-layer contribution of the $|\mathcal{V}_{\sigma^z}(\omega,\alpha)|$ response (top frame) for the *alt* structure as a function of the polarization angle $\alpha$ for the energy fixed to 0.720 eV. The corresponding layered contributions for the $\mathcal{V}^{xz}(\omega,\alpha)$ and $\mathcal{V}^{zy}(\omega,\alpha)$ components are presented in the central and bottom frames.

of the system. The *up* structure is *more* non-centrosymmetric than the *alt* structure and then the response is quite larger.

## IV. CONCLUSIONS

We have performed an *ab initio* calculation for the SVI by one-photon absorption of linearly polarized light in the *up* and *alt* 2D hydrogenated graphene structures that and we made the calculation for the case when the spin is polarized in the $z$ direction or when the velocity is directed along $x$ or $y$; this effect does not seem to have been reported previously. This SVI is very sensitive to the symmetry characteristics of the structures presenting an anisotropic behavior. We found that the *up* structure has the most intense response resulting in $|\mathcal{V}_{\sigma^z}(\omega,\alpha)| = 95.8\,\text{Km/s}$ and $|\mathcal{V}^{y}(\omega,\alpha)| = 87.9\,\text{Km/s}$ for an energy of the incoming beam of 0.088 eV. Also the response of the *alt* structure is comparable to the response of GaAs and CdSe bulk semiconductors. The spin relaxation time in pure and doped graphene is long enough in the order from nanoseconds to milliseconds.[39,40] The, according to our results the *alt* structure is a good candidate and the *up* structure an excellent candidate for the development of spintronics devices that require PSC due to the high spin velocity transport. The fact that the *up* structure is better than the *alt* structure comes from the symmetry: the first one is *more* non-centrosymmetric than the second resulting in a more intense response of the system.

## V. ACKNOWLEDGMENT

This work has been supported by *Consejo Nacional de Ciencia y Tecnología* (CONACyT), México, Grant No. 153930.

### Appendix A: Math derivation of $\dot{K}$

We give explicit expressions for the quantities used in the evaluation of Eq. (7); when appropriate, some intermediate steps are given for their derivation.

From Eq. (4) and Eq. (6), using $\mathbf{r}_{nm}(-\mathbf{k}) = \mathbf{r}_{mn}(\mathbf{k})$ and taking $\epsilon \to 0$, we have

$$
\begin{aligned}
\dot{K}^{\mathrm{ab}} &= \frac{e^2}{i\hbar^2}\int\frac{d^3k}{8\pi^3}\sum_{vcc'}K^{\mathrm{ab}}_{c'c}r^{\mathrm{c}}_{cv}r^{\mathrm{d}}_{vc'}\left(\frac{1}{\omega-\omega_{c'v}-i\epsilon}-\frac{1}{\omega-\omega_{cv}+i\epsilon}\right)E^{\mathrm{c}}(\omega)E^{\mathrm{d}*}(\omega)\\
&= \frac{e^2}{i\hbar^2}\int\frac{d^3k}{8\pi^3}\sum_{vcc'}\left((K^{\mathrm{ab}}_{c'c}r^{\mathrm{c}}_{cv}r^{\mathrm{d}}_{vc'})\big|_{\mathbf{k}>0}+(K^{\mathrm{ab}}_{c'c}r^{\mathrm{c}}_{cv}r^{\mathrm{d}}_{vc'})\big|_{\mathbf{k}<0}\right)\\
&\times\left(\frac{1}{\omega-\omega_{c'v}-i\epsilon}-\frac{1}{\omega-\omega_{cv}+i\epsilon}\right)E^{\mathrm{c}}(\omega)E^{\mathrm{d}*}(\omega)\\
&= \frac{e^2}{i\hbar^2}\int_{\mathbf{k}>0}\frac{d^3k}{8\pi^3}\sum_{vcc'}\left(K^{\mathrm{ab}}_{c'c}r^{\mathrm{c}}_{cv}r^{\mathrm{d}}_{vc'}+K^{\mathrm{ab}*}_{c'c}r^{\mathrm{c}}_{vc}r^{\mathrm{d}}_{c'v}\right)\\
&\times\left(\frac{1}{\omega-\omega_{c'v}-i\epsilon}-\frac{1}{\omega-\omega_{cv}+i\epsilon}\right)E^{\mathrm{c}}(\omega)E^{\mathrm{d}*}(\omega)\\
&= \frac{e^2}{i\hbar^2}\int_{\mathbf{k}>0}\frac{d^3k}{8\pi^3}\sum_{vcc'}\left(K^{\mathrm{ab}}_{c'c}r^{\mathrm{c}}_{cv}r^{\mathrm{d}}_{vc'}+(K^{\mathrm{ab}}_{c'c}r^{\mathrm{c}}_{cv}r^{\mathrm{d}}_{vc'})^*\right)\\
&\times\left(\frac{1}{\omega-\omega_{c'v}-i\epsilon}-\frac{1}{\omega-\omega_{cv}+i\epsilon}\right)E^{\mathrm{c}}(\omega)E^{\mathrm{d}*}(\omega)\\
&= \frac{e^2}{i\hbar^2}\frac{1}{2}\int\frac{d^3k}{8\pi^3}\sum_{vcc'}2\mathrm{Re}\Big[K^{\mathrm{ab}}_{c'c}r^{\mathrm{c}}_{cv}r^{\mathrm{d}}_{vc'}\Big]\Big\{\mathcal{P}\left(\frac{\omega_{c'c}}{(\omega-\omega_{c'v})(\omega-\omega_{cv})}\right)\\
&+i\pi\left(\delta(\omega-\omega_{c'v})+\delta(\omega-\omega_{cv})\right)\Big\}E^{\mathrm{c}}(\omega)E^{\mathrm{d}*}(\omega)\\
&\approx \frac{\pi e^2}{\hbar^2}\int\frac{d^3k}{8\pi^3}\sum_{vcc'}\mathrm{Re}\Big[K^{\mathrm{ab}}_{c'c}r^{\mathrm{c}}_{cv}r^{\mathrm{d}}_{vc'}\Big]\Big(\delta(\omega-\omega_{c'v})+\delta(\omega-\omega_{cv})\Big)E^{\mathrm{c}}(\omega)E^{\mathrm{d}*}(\omega)\\
&= \frac{\pi e^2}{\hbar^2}\int\frac{d^3k}{8\pi^3}\sum_{vcc'}\mathrm{Re}\Big[K^{\mathrm{ab}}_{c'c}r^{\mathrm{c}}_{cv}r^{\mathrm{d}}_{vc'}+K^{\mathrm{ab}}_{cc'}r^{\mathrm{c}}_{c'v}r^{\mathrm{d}}_{vc}\Big]\delta(\omega-\omega_{cv})E^{\mathrm{c}}(\omega)E^{\mathrm{d}*}(\omega),
\end{aligned}
\tag{A1}
$$

since $\omega_{cc'}\sim 0$ and we exchange $c\leftrightarrow c'$. Now, from Eq. (6) we obtain that

$$
\begin{aligned}
\mathrm{Re}\left[K^{\mathrm{ab}}_{cc'}r^{\mathrm{c}}_{c'v}r^{\mathrm{d}}_{vc}\right] =& \frac{1}{2}\left(K^{\mathrm{ab}}_{cc'}r^{\mathrm{c}}_{c'v}r^{\mathrm{d}}_{vc}+(K^{\mathrm{ab}}_{cc'}r^{\mathrm{c}}_{c'v}r^{\mathrm{d}}_{vc})^*\right)\\
=& \frac{1}{2}\left(K^{\mathrm{ab}}_{cc'}r^{\mathrm{c}}_{c'v}r^{\mathrm{d}}_{vc}+(K^{\mathrm{ab}}_{cc'}r^{\mathrm{c}}_{vc'}r^{\mathrm{d}}_{cv})\right)\\
=& \mathrm{Re}\left[K^{\mathrm{ab}}_{cc'}r^{\mathrm{c}}_{vc'}r^{\mathrm{d}}_{cv}\right]
\end{aligned}
\tag{A2}
$$

and then, Eq. (A1) can be written as

$$
\begin{aligned}
\dot{K}^{\mathrm{ab}} =& \frac{\pi e^2}{\hbar^2}\int\frac{d^3k}{8\pi^3}\sum_{vcc'}\mathrm{Re}\left[K^{\mathrm{ab}}_{c'c}r^{\mathrm{c}}_{cv}r^{\mathrm{d}}_{vc'}+K^{\mathrm{ab}}_{cc'}r^{\mathrm{c}}_{vc'}r^{\mathrm{d}}_{cv}\right]\delta(\omega-\omega_{cv})E^{\mathrm{c}}(\omega)E^{\mathrm{d}*}(\omega)\\
=& \frac{\pi e^2}{\hbar^2}\int\frac{d^3k}{8\pi^3}\sum_{vcc'}\mathrm{Re}\left[K^{\mathrm{ab}}_{c'c}\left(r^{\mathrm{c}}_{cv}r^{\mathrm{d}}_{vc'}+r^{\mathrm{c}}_{vc'}r^{\mathrm{d}}_{cv}\right)\right]\delta(\omega-\omega_{cv})E^{\mathrm{c}}(\omega)E^{\mathrm{d}*}(\omega)\\
=& \frac{\pi e^2}{\hbar^2}\int\frac{d^3k}{8\pi^3}\sum_{vcc'}\mathrm{Re}\left[K^{\mathrm{ab}}_{c'c}\left(r^{\mathrm{c}}_{cv}r^{\mathrm{d}}_{vc'}+(\mathrm{c}\leftrightarrow\mathrm{d})\right)\right]\delta(\omega-\omega_{cv})E^{\mathrm{c}}(\omega)E^{\mathrm{d}*}(\omega)\\
=& \frac{\pi e^2}{\hbar^2}\int\frac{d^3k}{8\pi^3}\sum_{vcc'}\mathrm{Re}\left[K^{\mathrm{ab}}_{c'c}\left(r^{\mathrm{c}}_{vc'}r^{\mathrm{d}}_{cv}+(\mathrm{c}\leftrightarrow\mathrm{d})\right)\right]\delta(\omega-\omega_{cv})E^{\mathrm{c}}(\omega)E^{\mathrm{d}*}(\omega)
\end{aligned}
\tag{A3}
$$

[1] S. A. Wolf, D. D. Awschalom, R. A. Buhrman, J. M. Daughton, S. Von Molnar, M. L. Roukes, A. Y. Chtchelkanova, and D. M. Treger, Science **294**, 1488 (2001).

[2] J. Fabian, A. Matos-Abiague, C. Ertler, P. Stano, and I. Zutic, Ac. Phys. Slov. (2007).

[3] D. D. Awschalom and M. E. Flatté, Nat. Phys. **3**, 153 (2007).

[4] S. Majumdar, R. Laiho, P. Laukkanen, I. J. Väyrynen, H. S. Majumdar, and R. Österbacka, App. Phys. Lett. **89**, 122114 (2006).

[5] S. Datta and B. Das, App. Phys. Lett. **56**, 665 (1990).

[6] M. Götte, M. Joppe, and T. Dahm, Scientific Reports **6** (2016).

[7] Y. V. Pershin and M. Di Ventra, Phys. Rev. B **78**, 113309 (2008).

[8] D. D. Awschalom, D. Loss, and N. Samarth, *Semiconductor Spintronics and Quantum Computation* (Springer Science & Business Media, 2013).

[9] S. Murakami, N. Nagaosa, and S. C. Zhang, Science **301**, 1348 (2003).

[10] A. Malshukov, C. Tang, C. Chu, and K.-A. Chao, Phys. Rev. B **68**, 233307 (2003).

[11] J. Sinova, D. Culcer, Q. Niu, N. A. Sinitsyn, T. Jungwirth, and A. H. MacDonald, Phys. Rev. Lett. **92**, 126603 (2004).

[12] R. D. R. Bhat and J. E. Sipe, Phys. Rev. Lett. **85**, 5432 (2000).

[13] A. Najmaie, R. D. R. Bhat, and J. E. Sipe, Phys. Rev. B **68**, 165348 (2003).

[14] R. D. R. Bhat, F. Nastos, A. Najmaie, and J. E. Sipe, Phys. Rev. Lett. **94**, 096603 (2005).

[15] H. Zhao, E. J. Loren, H. M. Van Driel, and A. L. Smirl, Phys. Rev. lett. **96**, 246601 (2006).

[16] M. J. Stevens, A. L. Smirl, R. D. R. Bhat, A. Najmaie, J. E. Sipe, and H. M. Van Driel, Phys. Rev. Lett. **90**, 136603 (2003).

[17] T. Kimura, N. Hashimoto, S. Yamada, M. Miyao, and K. Hamaya, NPG Asia Mat. **4**, e9 (2012).

[18] H. B. Heersche, P. Jarillo-Herrero, J. B. Oostinga, L. M. K. Vandersypen, and A. F. Morpurgo, Nature **446**, 56 (2007).

[19] A. Geim and K. Novoselov, Nat. Mater. **6**, 183 (2007).

[20] A. Reina, X. Jia, J. Ho, D. Nezich, H. Son, V. Bulovic, M. Dresselhaus, and J. Kong, Nano Lett. **9**, 30 (2008).

[21] K. S. Novoselov, Z. Jiang, Y. Zhang, S. V. Morozov, H. L. Stormer, U. Zeitler, J. C. Maan, G. S. Boebinger, P. Kim, and A. K. Geim, Science **315**, 1379 (2007).

[22] A. Balandin, S. Ghosh, W. Bao, I. Calizo, D. Teweldebrhan, F. Miao, and C. Lau, Nano Lett. **8**, 902 (2008).

[23] Y. Zhang, T. Tang, C. Girit, Z. Hao, M. Martin, A. Zettl, M. Crommie, Y. Shen, and F. Wang, Nature **459**, 820 (2009).

[24] M. Han, B. Özyilmaz, Y. Zhang, and P. Kim, Phys. Rev. Lett. **98**, 206805 (2007).

[25] Z. Ni, T. Yu, Y. Lu, Y. Wang, Y. P. Feng, and Z. Shen, ACS Nano **2**, 2301 (2008).

[26] D. Wei, Y. Liu, Y. Wang, H. Zhang, L. Huang, and G. Yu, Nano lett. **9**, 1752 (2009).

[27] B. Guo, L. Fang, B. Zhang, and J. R. Gong, Ins. J. **1**, 80 (2011).

[28] C. Coletti, C. Riedl, D. S. Lee, B. Krauss, L. Patthey, K. von Klitzing, J. H. Smet, and U. Starke, Phys. Rev. B **81**, 235401 (2010).

[29] A. Varykhalov, M. R. Scholz, T. K. Kim, and O. Rader, Phys. Rev. B **82**, 121101 (2010).

[30] D. C. Elias, R. R. Nair, T. M. G. Mohiuddin, S. V. Morozov, P. Blake, M. P. Halsall, A. C. Ferrari, D. W. Boukhvalov, M. I. Katsnelson, A. K. Geim, and K. S. Novoselov, Science **323**, 610 (2009).

[31] N. P. Guisinger, G. M. Rutter, J. N. Crain, P. N. First, and J. A. Stroscio, Nano Lett. **9**, 1462 (2009).

[32] D. K. Samarakoon and X. Q. Wang, ACS Nano **4**, 4126 (2010).

[33] R. Zapata-Peña, S. M. Anderson, B. S. Mendoza, and A. I. Shkrebtii, physica status solidi (b) **253**, 226 (2016).

[34] S. F. Alvarado, H. Riechert, and N. E. Christensen, Phys. Rev. Lett. **55**, 2716 (1985).

[35] B. Schmiedeskamp, B. Vogt, and U. Heinzmann, Phys. Rev. Lett. **60**, 651 (1988).

[36] N. Arzate, R. A. Vázquez-Nava, and B. S. Mendoza, Phys. Rev. B **90**, 205310 (2014).

[37] X. Gonze, B. Amadon, P. M. Anglade, J. M. Beuken, F. Bottin, P. Boulanger, F. Bruneval, D. Caliste, R. Caracas, M. Côté, T. Deutsch, L. Genovese, P. Ghosez, M. Giantomassi, S. Goedecker, D. Hamann, P. Hermet, F. Jollet, G. Jomard, S. Leroux, M. Mancini, S. Mazevet, M. Oliveira, G. Onida, Y. Pouillon, T. Rangel, G.-M. Rignanese, D. Sangalli, R. Shaltaf, M. Torrent, M. Verstraete, G. Zerah, and J. Zwanziger, Comput. Phys. Commun. **180**, 2582 (2009).

[38] C. Hartwigsen, S. Goedecker, and J. Hutter, Phys. Rev. B **58**, 3641 (1998).

[39] M. Wojtaszek, I. J. Vera-Marun, T. Maassen, and B. J. van Wees, Phys. Rev. B **87**, 081402 (2013).

[40] C. Ertler, S. Konschuh, M. Gmitra, and J. Fabian, Phys. Rev. B **80**, 041405 (2009).